ADVANCED ENERGY MATERIALS
www.advenergymat.de

WO_{3-x}/MoO_{3-x} Core/Shell Nanowires on Carbon Fabric as an Anode for All-Solid-State Asymmetric Supercapacitors

Xu Xiao, Tianpeng Ding, Longyan Yuan, Yongqi Shen, Qize Zhong, Xianghui Zhang, Yuanzhi Cao, Bin Hu, Teng Zhai, Li Gong, Jian Chen, Yexiang Tong, Jun Zhou, and Zhong Lin Wang*

Owing to the rapidly growing global energy consumption, the development of high-performance power sources has become an urgent and increasing demand in various fields such as portable electronics and sensor networks.[1–3] As a result of their excellent characteristics, such as superior power density, fast charge/discharge rates, and long cycle lifetime, supercapacitors (SCs, also known as electrochemical capacitors or ultracapacitors), which bridge the gap between high specific energy batteries and high specific power conventional capacitors, have been employed as state-of-the-art energy storage systems and widely used in consumer electronics, backup power sources, and pacemakers.[4–7]

Since the energy density is proportional to the capacitance (specific or areal capacitance), C, and square of the cell voltage, ΔU, which can be calculated as

$$E = 0.5C(\Delta U)^2 \quad (1)$$

an enhancement of energy density can be achieved by maximizing the capacitance and/or the operating voltage of SCs.[8] Compared with carbon-based materials, pseudo-capacitive materials such as transition metal oxides and conducting polymers[9–13] show much higher capacitive performance. Although the use of an organic electrolyte is one possible approach to increasing the operating voltage up to 4 V,[14–16] poor ionic conductivity will result in high equivalent series resistance (ESR) and low power output. Alternatively, asymmetric supercapacitors (ASCs) provide an environmentally friendly and effective approach to improving the energy density of SCs, as the operating voltage can be broadened by combining two appropriate electrodes with different potential windows.[8,17–19] For safety, weight, and environmental reasons, a solid-state electrolyte is superior to a liquid one, and is greatly desired for portable and wearable consumer electronics.

Many metal oxide negative electrode materials, such as molybdenum oxide (MoO_{3-x})[20] and iron oxide,[21] show a superior performance to carbon-based materials. However, the low electronic conductivity of metal oxides profoundly affects their electrochemical performance. In order to solve this problem, the use of high-specific-area and high-conductivity nanomaterials, such as zinc oxide and tungsten oxide (WO_{3-x}) nanowires,[12] as a scaffold to load electrochemically active materials is proposed as a viable solution.[22] Polyaniline (PANI) could be a positive electrode material because of its high capacitive performance and simple synthesis method. In this Communication, we report a simple and efficient method of growing MoO_{3-x}/WO_{3-x} core/shell nanowires on carbon fabric as a negative electrode, assembled with PANI nanowires on carbon fabric as a positive electrode, to fabricate high performance all-solid-state ASCs with H_3PO_4/poly(vinyl alcohol) (PVA) as the electrolyte. Electrochemical measurements indicated that the fabricated ASCs can be cycled reversibly between 0 and 1.9 V. Furthermore, the whole cell (including electrodes, separator, and electrolyte) exhibits a high areal capacitance of 216 mF cm^{-2}, and an energy density of 0.0019 Wh cm^{-3} at 2 mA cm^{-2}.

The WO_{3-x} nanowires were grown on carbon fabric by a catalyst-free, physical evaporation deposition process.[23] **Figure 1**a shows a scanning electron microscopy (SEM) image of WO_{3-x} nanowires grown radially on carbon fabric. A thin layer of MoO_{3-x} was coated on the surface of the WO_{3-x} nanowires by a simple electrodeposition method. Figure 1b shows a typical SEM image of MoO_{3-x}/WO_{3-x} core/shell nanostructures after 10 s MoO_{3-x} deposition. The MoO_{3-x}/WO_{3-x} core/shell nanostructures formed without any fracture of the WO_{3-x} nanowires, demonstrating the feasibility and efficiency of anodic electrodeposition. Typical transmission electron microscopy (TEM) images of MoO_{3-x}/WO_{3-x} core/shell nanostructures are shown in Figures 1c–e. According to the low-resolution TEM image, the MoO_{3-x} shell was homogeneous with a thickness of ~18 nm. In contrast to the single-crystalline core of WO_{3-x} (Figure 1f), the MoO_{3-x} shell was amorphous. The detailed chemical composition was probed by X-ray photoelectron spectroscopy (XPS),

X. Xiao, T. P. Ding, Dr. L. Y. Yuan, Y. Q. Shen, Q. Z. Zhong, X. H. Zhang, Y. Z. Cao, Prof. B. Hu, Prof. J. Zhou
Wuhan National Laboratory for Optoelectronics (WNLO), College of Optoelectronic Science and Engineering
Huazhong University of Science and Technology (HUST)
Wuhan 430074, P.R. of China
E-mail: jun.zhou@mail.hust.edu.cn
T. Zhai, Prof. Y. X. Tong
School of Chemistry and Chemical Engineering
Sun Yat-sen University
Guangzhou 510275, P.R. of China
L. Gong, Prof. J. Chen
Instrumental Analysis & Research Center
Sun Yat-sen University
Guangzhou 510275, P.R. of China
Prof. Z. L. Wang
School of Materials Science and Engineering
Georgia Institute of Technology
Atlanta, GA 30332-0245, USA

DOI: 10.1002/aenm.201200380

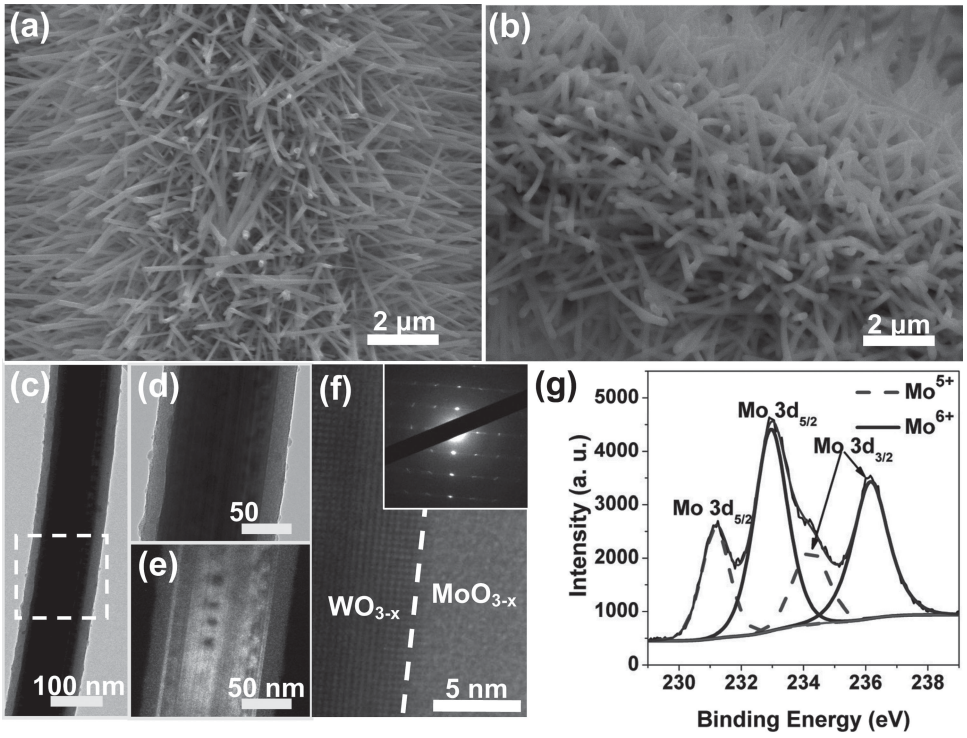

Figure 1. a,b) SEM images of WO_{3-x} nanowires grown on carbon fabric before (a) and after (b) MoO_{3-x} coating. c) Low-magnification TEM image of a MoO_{3-x} coated WO_{3-x} nanowire. d,e) Bright- (d) and dark-field (e) TEM images of a selected area. f) High-magnification TEM image of a MoO_{3-x} coated WO_{3-x} nanowire. g) XPS spectrum of Mo 3d level.

as shown in Figure S1 (Supporting Information) and Figure 1g. Among the W 4f peaks (Figure S1b), two strong peaks, corresponding to W^{6+}, and two medium peaks, corresponding to W^{5+}, were found, as expected. Another peak, at 40.35 eV, corresponded to Mo 4p. Figure 1g shows the XPS spectrum of Mo 3d, in which two strong peaks, corresponding to Mo^{6+}, and two medium peaks, corresponding to Mo^{5+}, were found.

It is well accepted that the conductivity and mass loading have a great impact on the electrochemical behavior of active materials.[24,25] A series of experiments with different deposition times of 10, 20, and 30 s were conducted to adjust the MoO_{3-x} growth parameters (the mass loading of MoO_{3-x} was about 1.34, 2.2, and 3 mg for deposition times of 10, 20, and 30 s, respectively). The electrochemical properties were characterized by a three-electrode configuration with 0.5 M Na_2SO_4 aqueous solution as the electrolyte, a graphite rod as the counter electrode, and a Ag/AgCl electrode as the reference electrode. According to the cyclic voltammetry (CV) scans at a scan rate of 100 mV s^{-1} (**Figure 2**a), the area enclosed by the CV curves increased with deposition time. Figure 2b shows typical galvanostatic charge/discharge curves at 3 mA cm^{-2} for the fabricated WO_{3-x}/MoO_{3-x} electrode with different deposition times, from which we can see that the discharge time increased with the deposition time. The areal capacitance for different MoO_{3-x} deposition times is plotted versus the discharge current in Figure 2f. The areal capacitance of a single electrode is given by

$$C = I\Delta t/\Delta E \quad (2)$$

$$C_a = C/S = I\Delta t/S\Delta E \quad (3)$$

where C is the total capacitance, I the discharge current, Δt the discharge time, ΔE the potential window during the discharge process after IR drop (R is resistance), and S the working area of the electrodes. The areal capacitance increases with MoO_{3-x} mass loading, and the highest areal capacitance of about 500 mF cm^{-2}, which is much higher than those reported in the literature (0.4–30 mF cm^{-2}),[16,26,27] was obtained for a deposition time of ca. 30 s. However, the mass of the MoO_{3-x} increased with deposition time as mentioned; thus lower conductivity may be obtained from thicker MoO_{3-x} shells. This hypothesis was confirmed by electrochemical impedance spectroscopy (EIS) measurements, as shown in Figure 2 c, in which the ESR was much larger for samples with deposition times of 20 s (3.5 Ω cm^2) and 30 s (3.7 Ω cm^2) than for the sample with 10 s deposition time (0.9 Ω cm^2). From considerations of peak power density (which is inversely proportional to the resistance of the cell), the sample with 10 s deposition time would be the best candidate for practical applications. Detailed characterization of 10 s deposition WO_{3-x}/MoO_{3-x} core/shell nanostructures was performed by CV scans and galvanostatic charge/discharge, the results of which are displayed in Figures 2d and e. The CV scans exhibited a roughly rectangular shape approximately symmetrical about the zero-current line even at a high scan rate of 200 mV s^{-1} (Figure 2d). In addition, the charging curves in the galvanostatic charge/discharge characterization shown in Figure 2e are almost symmetrical to the corresponding discharge curves, as well as exhibiting good linear voltage–time profiles, both of which indicate good capacitive behavior.

In order to fabricate all-solid-state ASCs with WO_{3-x}/MoO_{3-x} hybrid negative electrodes, we selected PANI grown on carbon

DOI: 10.1002/aenm.201200380

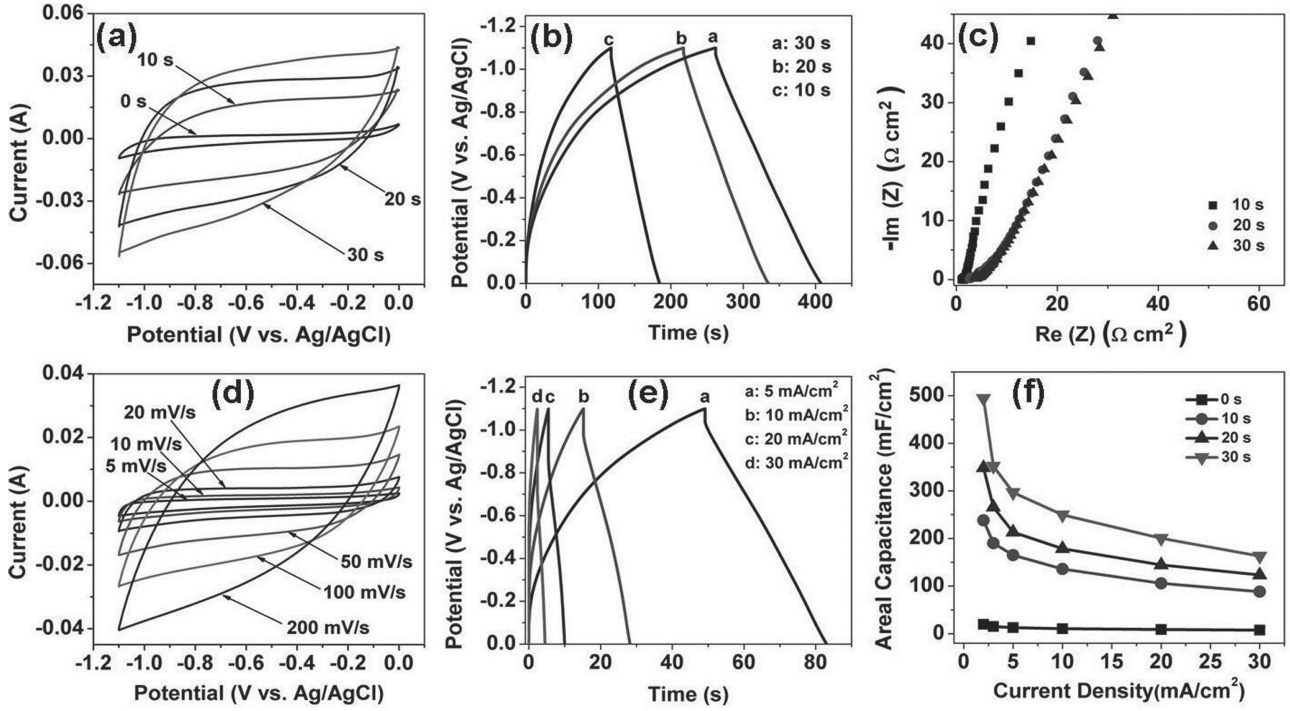

Figure 2. Electrochemical performance. a–c) CV scans (a), galvanostatic charge/discharge curves (b), and Nyquist plots (c) for MoO_{3-x} deposited on WO_{3-x} nanowires for different times. d,e) CV scans (d) and galvanostatic charge/discharge curves (e) for a WO_{3-x}/MoO_{3-x} nanostructure with deposition time 10 s. f) Areal capacitance as a function of current density for WO_{3-x}/MoO_{3-x} nanostructures with different deposition times. The area of each sample was 1 cm^2.

fabric as the positive electrode because of its high capacitive performance and simple synthesis method. In our experiment, PANI nanowires on carbon fabric were fabricated by a two-step electrodeposition method.[26] It should be noted that in order to take advantage of the largest voltage window, the areal capacitance between the positive and the negative electrodes should be adjusted according to

$$Q = C_a S \Delta E \tag{4}$$

$$Q^+ = Q^- \tag{5}$$

$$S^+ = S^- \tag{6}$$

$$C_a^+ / C_a^- = \Delta E^- / \Delta E^+ \tag{7}$$

where Q is the charge stored in the electrode, C_a the areal capacitance of the electrodes, S the working area of the electrodes, ΔE the potential window, and the superscripts "+" and "–" indicate the positive and negative electrodes, respectively. The morphology and detailed electrochemical characterization of the PANI electrode are presented in the Supporting Information (Figures S2 and S3). The CV scans of the fabricated all-solid-state ASCs at a stable potential window up to 1.9 V are shown in **Figure 3**a. Figure S4a (Supporting Information) presents a galvanostatic charge/discharge test at an operating voltage of 0–1.9 V; the good symmetry of the curves shows the good capacitive behavior.

Based on the galvanostatic charge/discharge curves, the areal capacitance of the fabricated ASCs could be calculated using Equations 2 and 3, where C is the total capacitance of the device and S the working area of the device. The highest areal capacitance was ~216 mF cm^{-2} at 2 mA cm^{-2} discharge current, which is much larger than those reported in the literature at the same discharge current,[8,16,27] and ~130 mF cm^{-2} still remained at 20 mA cm^{-2} discharge current (Figure 3b). The ESR of the as-fabricated ASCs was 30 Ω cm^2 (Figure S4b, Supporting Information). Furthermore, as a power source operated at large discharge current with high power density, the cyclic stability of ASCs is significantly important. As can be seen in Figure 3d, the fabricated ASC showed a good cyclic stability in the voltage window of 0 to 1.9 V at a large galvanostatic current of 5 mA cm^{-2} over 10000 cycles. After 10000 cycles 75% of the capacitance was retained; the degradation may be caused by the combination of the effect of delamination of active materials owing to ion insertion and insufficient sealing of the device.[28] A Ragone plot showing the energy density as a function of average power density of the fabricated all-solid-state ASCs can be seen in Figure 3c. Since the total weight and volume are very important factors for practical applications, the energy density and average power density were calculated with the total weight or volume for commercial SCs. Accordingly, the energy density and average power density of the cell were calculated using

$$E = 0.5C(\Delta U)^2 / V \tag{8}$$

$$P = 3600E / \Delta t \tag{9}$$

where C is the total capacitance of the cell that can be achieved according to Equation 2, ΔU is the cell voltage, V is the volume of the cell including the electrodes, separators, and electrolyte,

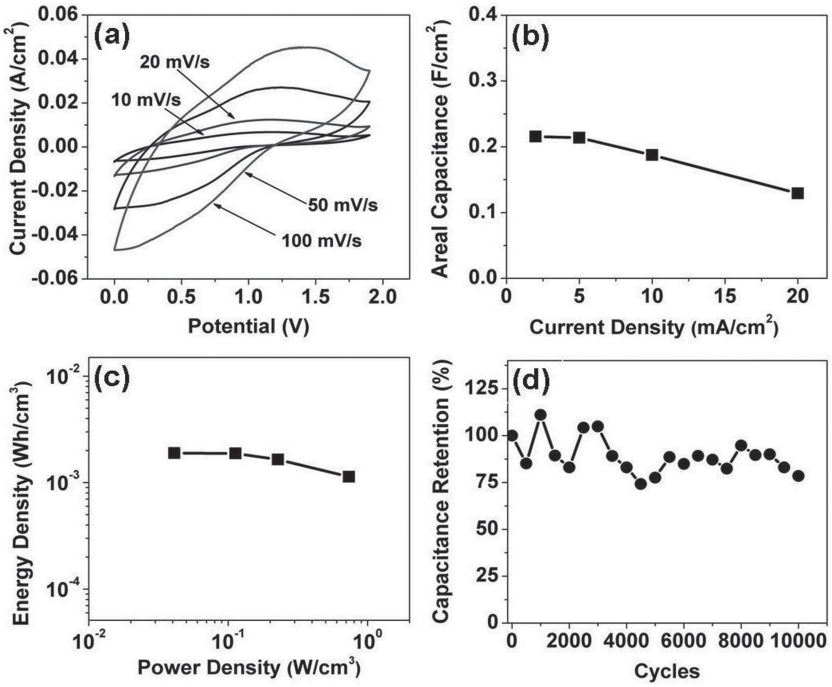

Figure 3. a) CV scans of all-solid-state ASCs at different scan rates. b) Areal capacitance of the fabricated all-solid-state ASCs as a function of discharge current density. c) Ragone plot of fabricated all-solid-state ASCs. d) Cycle life of an ASC.

and Δt is the discharge time. The fabricated all-solid-state ASCs (the volume of the whole cell was about 0.057 cm^3) exhibited a high energy density of 0.0019 Wh cm^{-3}, which is about twice that of graphene oxide (8×10^{-4} Wh cm^{-3}) and onion-like carbon SCs (1×10^{-3} Wh cm^{-3}).[29,30] Besides, power density of 0.73 W cm^{-3} was obtained while the energy density was still 0.0011 Wh cm^{-3} at 20 mA cm^{-2} discharge current. This high rate capability demonstrated a great performance potential for energy storage applications. In addition, the mass of the fabricated SC was only about 115 mg, including all the components, which makes it suitable as a power source for portable electronics. After being charged to 3.8 V, two all-solid-state ASCs connected in series were able to power a blue light-emitting device (LED; see the inset of Figure S4b in the Supporting Information).

SCs could be charged by sustainable and renewable sources and drive electronic devices continually, forming a self-powered system.[3,31] We used a solar cell to charge the all-solid-state ASCs and then drive an infrared sensor system to verify the feasibility of a self-powered system. **Figure 4**a is the schematic of the ACS-driven infrared sensor system. The infrared-emitting diode (IED, L1) was driven by a direct current power source (DS345), which could output a square signal (Figure S5, Supporting Information). Two all-solid-state ASCs connected in series were charged by a solar cell to 3.6 V (Figure S6, Supporting Information) and were used to drive an infrared receiver diode (IRD, L2). When the IRD received the signal from the IED, the resistance of the IRD decreased. Then the voltage of the commercial LED (L3) increased and it lit up (the lowest working voltage is 1.5 V). Figure 4b shows the voltage–time curve of the commercial LED. Since the IED was driven by a 0.5 Hz square signal, the voltage of the commercial LED changed at 0.5 Hz. When the IED was emitting, the LED lit up, demonstrating the feasibility of a self-powered sensor system driven by all-solid-state ASCs.

In summary, WO_{3-x}/MoO_{3-x} core/shell nanowires on carbon fabrics were fabricated and demonstrated as novel negative electrodes. When these were assembled with PANI positive

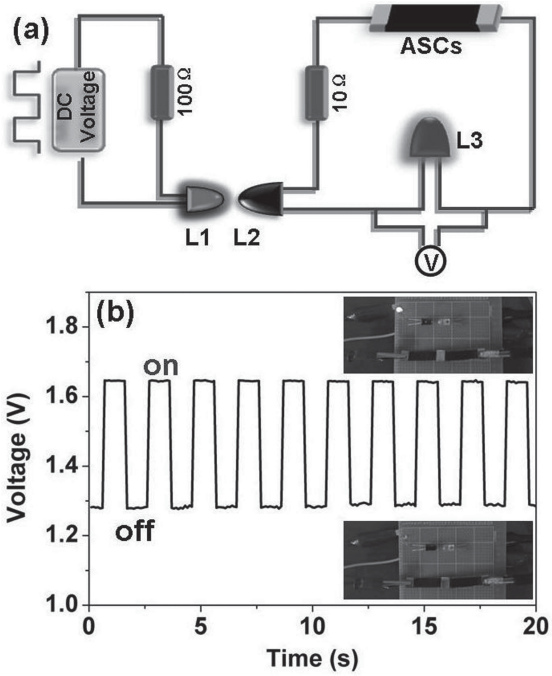

Figure 4. a) Schematic of the ACS-driven infrared sensor system. L1: IED. L2: IRD. L3: Commercial LED. b) Voltage–time curve of the commercial LED.

DOI: 10.1002/aenm.201200380

electrodes, flexible all-solid-state ASCs were fabricated, which exhibited stable performance between 0 and 1.9 V, a high areal capacitance of ca. 216 mF cm^{-2}, an energy density of 0.0019 Wh cm^{-3}, and high rate capability. By virtue of other great characteristics, such as low toxicity, flexibility, environmental compatibility, light weight, and low requirements for packaging, the fabricated all-solid-state ASCs displayed their potential for applications in energy storage, flexible electronics, and other consumer electronics.

Experimental Section

Synthesis of molybdenum oxide–coated WO_{3-x} nanostructure: All chemicals were analytical grade and were used without further purification. The WO_{3-x} nanowires were fabricated on both sides of carbon fabric strips by chemical vapor deposition at 1080 °C for 15 min in an oxygen atmosphere. Briefly, during the growth process, carbon fabric strips were positioned above the tungsten boat (120 mm × 20 mm × 0.3 mm) containing W powder (1 g, purity: 99.8%). A mixture of high-purity argon gas (99.999%) and oxygen gas (99.999%) with constant flow rates of 100 and 0.5 standard cubic centimeters per minute (sccm), respectively, were introduced into the chamber, keeping the pressure at ~100 Pa. An aqueous solution composed of 0.1 M sodium molybdate (Na_2MO_4), 0.1 M ethylenediamine tetraacetic acid disodium (Na_2EDTA), and 0.1 M ammonium acetate (CH_3COONH_4) was used to coat molybdenum oxide on the as-formed WO_{3-x} nanowires by an electrochemical deposition method at a constant voltage of –2 V at 70 °C.

Assembly of all-solid-state ASCs: A H_3PO_4/PVA gel electrolyte was simply prepared by mixing PVA powder (6 g), H_3PO_4 (6 g), and deionized water (60 mL) together. Then the mixture was heated to around 85 °C under vigorous stirring until the solution became clear. After the solution had cooled down, the molybdenum oxide–coated WO_{3-x} and PANI/carbon fabric electrodes were immersed for 5 min then assembled together and separated by a cellulose separator (NKK TF40, 40 μm). The carbon fabrics served as current collectors. The device was left in the fume hood at room temperature to vaporize the excess water.

Characterization: The morphology of the samples was probed by a high-resolution field emission scanning electron microscope (FEI Sirion 200) and a high-resolution field emission transmission electron microscope (TEM, JEOL JEM 2010-HR). The XPS measurement was performed on an ESCALab250 (Thermo Scientific). All the electrochemical measurements were carried out at room temperature using an Autolab PGSTAT302N (Metrohm AG) and CHI660D (CH Instruments), and the electrochemical impedance spectroscopy was performed in the frequency range from 10 mHz to 100 kHz with a potential amplitude of 10 mV. For the single electrode test, a piece of electrode (~0.7 cm × 1.5 cm) was dipped into 0.5 M Na_2SO_4 as the working electrode. A Ag/AgCl reference electrode and a carbon rod counter electrode were used in the measurement. The amount of deposited molybdenum oxide and PANI was measured by a microbalance (CPA225D, Sartorius) with an accuracy of 0.01 mg.

Supporting Information

Supporting Information is available from the Wiley Online Library or from the author.

Acknowledgements

This work was financially supported by the National Natural Science Foundation of China (51002056, 51072236), the National Basic Research Program of China (2012CB619302), the Foundation for the Authors of National Excellent Doctoral Dissertations of PR China (201035), the Program for New Century Excellent Talents in University (NCET-10-0397), and the Fundamental Research Funds for the Central Universities of China (2012NQ106). The authors acknowledge the Analysis and Testing Center of Huazhong University of Science and Technology (HUST) and the Optoelectronic Micro-nano Fabrication Facility of Wuhan National Laboratory for Optoelectronics (WNLO).

Received: May 28, 2012
Published online:

[1] A. Burke, *J. Power Sources* **2000**, *91*, 37.
[2] J. R. Miller, P. Simon, *Science* **2008**, *321*, 651.
[3] X. Xiao, L. Y. Yuan, J. W. Zhong, T. P. Ding, Y. Liu, Z. Cai, Y. Rong, H. W. Han, J. Zhou, Z. L. Wang, *Adv. Mater.* **2011**, *23*, 5440.
[4] P. Simon, Y. Gogotsi, *Nat. Mater.* **2008**, *7*, 845.
[5] B. E. Conway, *Electrochemical Supercapacitors: Scientific Fundamentals and Technological Applications*, Plenum, New York **1999**.
[6] J. M. Miller, B. Dunn, T. D. Tran, R. W. Pekala, *J. Electrochem. Soc.* **1997**, *144*, L309.
[7] A. Lewandowski, M. Galinski, *J. Power Sources* **2007**, *173*, 822.
[8] J. Zhang, J. Jiang, H. Li, X. S. Zhao, *Energy Environ. Sci.* **2011**, *4*, 4009.
[9] G. Yu, L. Hu, M. Vosgueritchian, H. Wang, X. Xie, J. R. McDonough, X. Cui, Y. Cui, Z. Bao, *Nano Lett.* **2011**, *11*, 2905.
[10] M. S. Wu, R. H. Lee, *J. Electrochem. Soc.* **2009**, *156*, A737.
[11] L. Y. Yuan, X. H. Lu, X. Xiao, T. Zhai, J. J. Dai, F. C. Zhang, B. Hu, X. Wang, L. Gong, J. Chen, C. G. Hu, Y. X. Tong, J. Zhou, Z. L. Wang, *ACS Nano* **2012**, *6*, 656.
[12] X. H. Lu, T. Zhai, X. H. Zhang, Y. Q. Shen, L. Y. Yuan, B. Hu, L. Gong, J. Chen, Y. H. Gao, J. Zhou, Y. X. Tong, Z. L. Wang, *Adv. Mater.* **2012**, *24*, 938.
[13] Y. Y. Horng, Y. C. Lu, Y. K. Hsu, C. C. Chen, L. C. Chen, K. H. Chen, *J. Power Sources* **2010**, *195*, 4418.
[14] T. Y. Kim, H. W. Lee, M. Stoller, D. R. Dreyer, C. W. Bielawski, R. S. Ruoff, K. S. Suh, *ACS Nano* **2010**, *5*, 436.
[15] A. Izadi-Najafabadi, S. Yasuda, K. Kobashi, T. Yamada, D. N. Futaba, H. Hatori, M. Yumura, S. Iijima, K. Hata, *Adv. Mater.* **2010**, *22*, E235.
[16] M. Kaempgen, C. K. Chan, J. Ma, Y. Cui, G. Gruner, *Nano Lett.* **2009**, *9*, 1872.
[17] Z. S. Wu, W. Ren, D. W. Wang, F. Li, B. Liu, H. M. Cheng, *ACS Nano* **2010**, *4*, 5835.
[18] P. C. Chen, G. Shen, Y. Shi, H. Chen, C. Zhou, *ACS Nano* **2010**, *4*, 4403.
[19] H. A. Andreas, B. E. Conway, *Electrochim. Acta* **2006**, *51*, 6510.
[20] G. R. Li, Z. L. Wang, F. L. Zheng, Y. N. Ou, Y. X. Tong, *J. Mater. Chem.* **2011**, *21*, 4217.
[21] M. S. Wu, Y. H. Ou, Y. P. Lin, *Electrochim. Acta* **2010**, *55*, 3240.
[22] C. Meng, C. Liu, L. Chen, C. Hu, S. Fan, *Nano Lett.* **2010**, *10*, 4025.
[23] X. Zhang, L. Gong, K. Liu, Y. Cao, X. Xiao, W. Sun, X. Hu, Y. Gao, J. Chen, J. Zhou, Z. L. Wang, *Adv. Mater.* **2010**, *22*, 5292.
[24] L. Hu, J. W. Choi, Y. Yang, S. Jeong, F. La Mantia, L. F. Cui, Y. Cui, *Proc. Natl. Acad. Sci. USA* **2009**, *106*, 21490.
[25] M. D. Stoller, R. S. Ruoff, *Energy Environ. Sci.* **2010**, *3*, 1294.
[26] L. Y. Yuan, X. Xiao, T. P. Ding, J. W. Zhong, X. H. Zhang, Y. Shen, B. Hu, Y. H. Huang, J. Zhou, Z. L. Wang, *Angew. Chem. Int. Ed.* **2012**, *51*, 4934.
[27] M. Pasta, F. La Mantia, L. B. Hu, H. D. Deshazer, Y. Cui, *Nano Res.* **2010**, *3*, 452.
[28] L. Hu, W. Chen, X. Xie, N. Liu, Y. Yang, H. Wu, Y. Yao, M. Pasta, H. N. Alshareef, Y. Cui, *ACS Nano* **2011**, *5*, 8904.
[29] D. Pech, M. Brunet, H. Durou, P. Huang, V. Mochalin, Y. Gogotsi, P.-L. Taberna, P. Simon, *Nat. Nanotechnol.* **2010**, *5*, 651.
[30] W. Gao, N. Singh, L. Song, Z. Liu, A. L. M. Reddy, L. Ci, R. Vajtai, Q. Zhang, B. Wei, P. M. Ajayan, *Nat. Nanotechnol.* **2011**, *6*, 496.
[31] Z. L. Wang, *Nano Today* **2010**, *5*, 512.